Published by

British Journal of Contemporary Research

BEXFORD PUBLISHING

Threshold Dynamics and Robust Control of Cassava Mosaic Disease in a Host–Vector System — Analytical Stability and a Framework for Stochastic Koopman-Based Forecasting

Original Research Article | Volume 1 | Issue 6 | 2026 | Article Number: 037

Accepted: 20 October 2026 | Published: 10 November 2026 | ISSN: 2979-8582 (Online)

Crossref : **https://doi.org/10.67693/BJCR-SBYPVDU3**

Napoleon Ifeakachukwu OCHONOGOR[1], Believe Igbunu AKPOBROKA[2]

[1]Department of Mathematics, Faculty of Science, Dennis Osadebay University, Asaba, Delta State, Nigeria

Correspondence: Napoleon Ifeakachukwu OCHONOGOR, napoloen.ochonogor@dou.edu.ng

Abstract

Cassava mosaic disease (CMD) is transmitted by infectious whiteflies and infected planting material. We investigate a deliberately reduced two-state host–vector model, derive its reproduction threshold and equilibria, and formulate robust transmission suppression under interval uncertainty. Positive invariance and global disease-free stability for $R_0 \leq 1$ are established analytically. Independently recomputed synthetic experiments examine subcritical, critical and supercritical trajectories, equilibrium branches and nine constrained control-allocation scenarios. For the illustrative baseline, $R_0 = 2$ and the endemic equilibrium is (0.5625, 0.4286). Worst-case control allocations enforce $R_c \leq 0.95$ under prescribed upper transmission bounds; optimal allocations depend strongly on relative effort weights. These results concern a stylised model rather than calibrated field dynamics. Infected-cutting introduction, heterogeneous whitefly ecology and empirical validation remain outside its scope. Stochastic dynamics and Koopman forecasting are identified as future research rather than completed results.

Keywords: Cassava Mosaic Disease, Host–Vector Dynamics, Basic Reproduction Number, Global Stability, Robust Control, Parameter Uncertainty, Stochastic Differential Equations, Koopman Operator, Extended Dynamic Mode Decomposition

© 2026 The Authors. Published by Bexford Publishing Ltd

1. INTRODUCTION

Cassava mosaic disease (CMD) is caused by cassava mosaic begomoviruses and spreads through infected stem cuttings and Bemisia tabaci whiteflies. The simultaneous operation of these transmission routes, cultivar variation and spatial dispersal makes the design of effective control strategies challenging [1, 3, 6]. Surveillance research also emphasizes consistent measurements of disease incidence, severity and whitefly abundance. Host–vector models provide interpretable threshold quantities but require careful specification of their biological assumptions.

Existing mechanistic CMD models already include infected-cutting introductions, reproduction-number analysis, global stability and intervention optimisation [3,13]. More detailed formulations address non-cassava reservoirs [2], stage-structured whiteflies and vector feeding preferences [4], and sensitivity-guided control [5,14]. Consequently, the present work does not claim priority for reproduction thresholds or Lyapunov analysis. Instead, it isolates the transparent effect of rectangular uncertainty on a reduced host–vector control constraint and independently tests the associated synthetic optimisation.

The objectives are to (i) establish the deterministic threshold and equilibrium results; (ii) derive worst-case transmission suppression conditions under fixed bounded uncertainty; (iii) verify candidate control allocations against feasibility and Karush–Kuhn–Tucker conditions; and (iv) provide reproducible numerical trajectories and parameter sweeps. Infected planting-material importation is intentionally excluded; therefore, the disease-free equilibrium is relevant only in the absence of exogenous infected introductions. No field-level forecast accuracy is asserted.

2. LITERATURE CONTEXT AND RESEARCH POSITIONING

2.1 CMD transmission and intervention modelling

Earlier CMD work has modelled both infected cuttings and whitefly infection and established stability and policy implications [3]. Subsequent work has incorporated alternative host plants [2], stage-specific vector development and feeding behaviour [4], and sensitivity-based intervention design [5]. Research on cassava production and pest management also stresses the broader crop-system context [6]. A recent vector–host cross-protection study further demonstrates that richer biological mechanisms can change bifurcation structure [13]. These studies are not interchangeable with the present two-state formulation: omission of cutting-mediated introduction and stage structure materially restricts biological interpretation. The contribution here is a tractable uncertainty-to-allocation calculation, not a general replacement for richer CMD models.

2.2 Stochastic modelling and Koopman methods

Stochastic and fractional-delay CMD frameworks have been investigated [7], while extended dynamic mode decomposition (EDMD) supplies a finite-dimensional approximation of Koopman evolution operators [8]. Neither stochasticity nor Koopman analysis automatically improves forecasts: diffusion coefficients must respect the feasible state space, and predictive skill must be tested on held-out time-ordered observations against mechanistic and persistence baselines. Spatial movement of planting material and vectors can also be consequential in mixed-mode crop disease transmission [14]. These aspects motivate future extensions, but they are not numerical findings of this paper.

2.3 Research gap and scope of novelty

The research gap addressed is narrow: how can rectangular uncertainty in effective host–vector transmission be converted into an auditable worst-case threshold and minimum-effort allocation for a normalized two-state system? Earlier CMD studies have already established much stronger

© 2026 The Authors. Published by Bexford Publishing Ltd

epidemiological models [3–5]; the present work contributes a reproducible methodological illustration rather than a claim of first-ever CMD robust control. Validation of uncertainty bounds, intervention effectiveness and field relevance remains essential.

2.4 Contributions and limitations

- Derivation of the reproduction threshold and explicit equilibrium expressions for a two-state normalized system.
- A global disease-free stability proof, including the threshold case $R_0 = 1$.
- A robust threshold condition for a rectangular uncertainty set and a constrained quadratic-effort allocation formulation.
- Synthetic numerical illustrations, clearly distinguished from empirical estimation.
- A proposed, not yet implemented, stochastic and EDMD research workflow.

3. DETERMINISTIC HOST–VECTOR MODEL

Let $x(t) \in [0,1]$ be the fraction of infected cassava plants and $y(t) \in [0,1]$ the fraction of infectious adult whiteflies at time t. The reduced system is [3, 2]

$$\frac{dx}{dt} = \beta_h(1 - x)y - \mu_h x,$$

$$\frac{dy}{dt} = \beta_v(1 - y)x - \mu_v y. \qquad (1)$$

The parameters β_h, β_v, μ_h and μ_v are strictly positive. The coefficients β_h and β_v are effective per-time transmission coefficients, not probabilities by themselves. The removal coefficients μ_h and μ_v represent aggregate turnover or loss processes in the normalized model. Host and vector totals are assumed constant. Infected planting-material introductions and seasonal vector recruitment are not represented.

3.1 Positivity and boundedness

Define $\Omega = [0,1]^2$. On the boundary $x = 0$, $dx/dt = \beta_h y \geq 0$; on $x = 1$, $dx/dt = -\mu_h < 0$. Similarly, on $y = 0$, $dy/dt = \beta_v x \geq 0$; on $y = 1$, $dy/dt = -\mu_v < 0$. The vector field is therefore inward-pointing or tangent on each boundary face. Since the right-hand side is polynomial and locally Lipschitz, every initial condition in Ω generates a unique solution that remains in Ω for all $t \geq 0$.

3.2 Disease-free equilibrium and reproduction number

The disease-free equilibrium is $E_0 = (0,0)$. The next-generation matrices at E_0 are

$$F = \begin{pmatrix} 0 & \beta_h \\ \beta_v & 0 \end{pmatrix}, \quad V = \begin{pmatrix} \mu_h & 0 \\ 0 & \mu_v \end{pmatrix}.$$

The basic reproduction number is the spectral radius of FV^{-1}:

$$R_0 = \rho\left(FV^{-1}\right) = \sqrt{\frac{\beta_h \beta_v}{\mu_h \mu_v}}. \qquad (2)$$

Thus R_0 is a threshold quantity for the reduced model. Its epidemiological interpretation depends on the model's normalization and on how the effective rates are estimated.

3.3 Endemic equilibrium

At equilibrium, the equations give $x = ay/(1 + ay)$ and $y = bx/(1 + bx)$, where $a = \beta_h/\mu_h$ and $b = \beta_v/\mu_v$. A positive equilibrium exists if and only if $ab > 1$, equivalently $R_0 > 1$. When it exists, it is unique and is

© 2026 The Authors. Published by Bexford Publishing Ltd

given by

$$x^* = \frac{ab-1}{b(1+a)}, \qquad y^* = \frac{ab-1}{a(1+b)}. \tag{3}$$

Both components lie strictly between zero and one when $ab > 1$. If $ab \leq 1$, no positive endemic equilibrium exists in the biological region.

3.4 Jacobian and local stability of the disease-free equilibrium

The Jacobian matrix of system (1) is

$$J(x,y) = \begin{pmatrix} -\beta_h y - \mu_h & -\beta_h(1-x) \\ \beta_v(1-y) & -\beta_v x - \mu_v \end{pmatrix}.$$

At the disease-free equilibrium,

$$J(E_0) = \begin{pmatrix} -\mu_h & -\beta_h \\ \beta_v & -\mu_v \end{pmatrix}.$$

The eigenvalues are

$$\lambda_{\pm} = -\frac{\mu_h+\mu_v}{2} \pm \frac{1}{2}\sqrt{(\mu_h-\mu_v)^2 + 4\beta_h\beta_v}.$$

An associated unnormalized eigenvector is $v_{\pm} = (\beta_h, \mu_h + \lambda_{\pm})^T$, whenever this representation is nonzero. The trace is $-(\mu_h + \mu_v) < 0$ and the determinant is $\mu_h\mu_v(1 - R_0^2)$. Therefore E_0 is locally asymptotically stable for $R_0 < 1$ and unstable for $R_0 > 1$. At $R_0 = 1$, one eigenvalue is zero and linearization alone is inconclusive.

3.5 Global disease-free stability

Theorem 1. The disease-free equilibrium E_0 is globally asymptotically stable in Ω for $R_0 \leq 1$.

Proof. Define the Lyapunov function $L(x,y) = \beta_v x + \mu_h y$. Since β_v and μ_h are positive, L is nonnegative on Ω and vanishes only at E_0. Along solutions of (1),

$$\frac{dL}{dt} = (\beta_h\beta_v - \mu_h\mu_v)y - \beta_v(\beta_h + \mu_h)xy. \tag{4}$$

If $R_0 \leq 1$, then $\beta_h\beta_v - \mu_h\mu_v \leq 0$, so $dL/dt \leq 0$. For $R_0 < 1$, equality in (4) requires $y = 0$. The only invariant subset of $y = 0$ is E_0, because $dy/dt = \beta_v x > 0$ whenever $x > 0$ and $y = 0$. At $R_0 = 1$, $dL/dt = -\beta_v(\beta_h + \mu_h)xy$; the largest invariant subset of the zero-derivative set $xy = 0$ is again E_0. The set Ω is compact and positively invariant, so LaSalle's invariance principle implies global asymptotic stability. □

3.6 Local stability of the endemic equilibrium

For $R_0 > 1$, the endemic equilibrium E^* is locally asymptotically stable. The trace of $J(E^*)$ is negative because all parameters and equilibrium components are positive. Using the equilibrium identities $\beta_h y^* = \mu_h x^*/(1 - x^*)$ and $\beta_v x^* = \mu_v y^*/(1 - y^*)$, the determinant can be written as

$$\det J(E^*) = \mu_h\mu_v\left[\frac{1}{(1-x^*)(1-y^*)} - 1\right] > 0. \tag{5}$$

For a two-dimensional system, negative trace and positive determinant imply that both eigenvalues have negative real parts. Hence E^* is locally asymptotically stable. This argument does not establish global asymptotic stability of E^*.

4. ROBUST TRANSMISSION UNCERTAINTY AND CONTROL

© 2026 The Authors. Published by Bexford Publishing Ltd

Suppose the effective transmission coefficients are uncertain but lie in fixed intervals $\beta_h \in [\beta_h^-, \beta_h^+]$ and $\beta_v \in [\beta_v^-, \beta_v^+]$, with positive endpoints. Let constant control intensities $u_h, u_v \in [0,1]$ reduce the effective transmission coefficients to $(1-u_h)\beta_h$ and $(1-u_v)\beta_v$. The controlled reproduction number is

$$R_c = \sqrt{\frac{(1-u_h)(1-u_v)\beta_h\beta_v}{\mu_h\mu_v}}. \quad (6)$$

4.1 Robust threshold proposition

Proposition 1. The disease-free equilibrium is locally asymptotically stable for every fixed admissible transmission pair if

$$(1-u_h)(1-u_v)\beta_h^+\beta_v^+ < \mu_h\mu_v. \quad (7)$$

If the left-hand side of (7) exceeds $\mu_h\mu_v$, the disease-free equilibrium is unstable for at least one admissible pair. At equality, the upper-corner linearization has a zero eigenvalue; nevertheless, global asymptotic stability follows for that fixed pair from the Lyapunov argument in Theorem 1, with the controlled transmission rates substituted.

Proof. The infected-state linearization is the Metzler matrix $A = [[-\mu_h, (1-u_h)\beta_h], [(1-u_v)\beta_v, -\mu_v]]$. Its trace is negative, and its determinant is $\mu_h\mu_v - (1-u_h)(1-u_v)\beta_h\beta_v$. It is Hurwitz precisely when this determinant is positive. The product $\beta_h\beta_v$ is increasing in each positive transmission coefficient, so its maximum over the uncertainty rectangle occurs at (β_h^+, β_v^+). The result follows. □

4.2 Robust global disease elimination

Corollary 1. Under the strict inequality (7), the disease-free equilibrium is globally asymptotically stable in Ω for each fixed admissible parameter pair.

Proof. For each admissible pair, A is Hurwitz and Metzler. Hence there exists a strictly positive vector w such that w^TA is componentwise negative. With $z = (x,y)^T$, the controlled nonlinear system has the form $\dot{z} = Az - (c_hxy, c_vxy)^T$, where $c_h = (1-u_h)\beta_h$ and $c_v = (1-u_v)\beta_v$ are nonnegative. The function $V = w^Tz$ is positive for every nonzero z in Ω, and $V = w^TAz - (w_1c_h + w_2c_v)xy < 0$ for $z \neq 0$. Thus V is a strict Lyapunov function on Ω and E_0 is globally asymptotically stable. □

4.3 Constrained effort-allocation problem

To maintain a prescribed worst-case safety margin, consider the quadratic objective

$$C(u_h, u_v) = c_h u_h^2 + c_v u_v^2. \quad (8)$$

subject to

$$(1-u_h)(1-u_v) \le \frac{(1-\varepsilon)^2\mu_h\mu_v}{\beta_h^+\beta_v^+},$$

$$0 \le u_h, u_v \le 0.95, \qquad \varepsilon = 0.05. \quad (9)$$

The margin $\varepsilon = 0.05$ is a design choice, not an empirically estimated safety factor. The coefficients c_h and c_v are hypothetical relative effort weights and are not monetary costs. The constraint ensures $R_c \le 0.95$ at the upper-corner transmission values.

© 2026 The Authors. Published by Bexford Publishing Ltd

4.4 Analytical check of the interior optimum

Let $q = (1 - \varepsilon)^2\mu_h\mu_v/(\beta_h^+\beta_v^+)$, $r = 1 - u_h$ and $s = 1 - u_v$. When the safety constraint is active and the optimum is interior, $rs = q$. The first-order condition for minimizing the quadratic objective becomes

$$c_h r(1 - r) = c_v s(1 - s). \tag{10}$$

Equation (10) supplies an independent check on numerical solutions. Any reported optimum should also be checked against the bound constraints and the Karush–Kuhn–Tucker conditions. Solver convergence by itself does not certify global optimality.

5. SYNTHETIC NUMERICAL EXPERIMENTS

All parameter values in this section are illustrative. They are not fitted to CMD observations, field measurements or intervention trials. The purpose is to verify internal consistency and demonstrate the consequences of the model assumptions.

5.1 Baseline parameterization

Parameter	Illustrative value	Interpretation
β□	0.60	Effective host-infection transmission coefficient
β_v	0.40	Effective vector-infection transmission coefficient
μ□	0.20	Host infected-state removal/turnover rate
μ_v	0.30	Infectious-vector removal/replacement rate
ε	0.05	Prespecified robust safety margin

For the baseline parameters, $R_0 = 2$ and $E^* = (0.562500, 0.428571)$. The disease-free Jacobian eigenvalues are 0.242443 and -0.742443. The independently recomputed endemic Jacobian is

$$J(E^*) \approx [[-0.457143, 0.262500], [0.228571, -0.525000]].$$

with eigenvalues -0.243784 and -0.738359 (order immaterial). These independently recomputed values confirm local asymptotic stability of E*.

5.2 Threshold behaviour and equilibrium response

Because R_0 depends on the product $\beta_h\beta_v$ and inversely on $\mu_h\mu_v$, increasing either transmission coefficient raises R_0, whereas increasing either removal coefficient lowers it. These monotonic statements follow algebraically from equation (2). The equilibrium prevalence responses can be plotted using equation (3),

© 2026 The Authors. Published by Bexford Publishing Ltd

with the disease-free branch used when $R_0 \leq 1$. Parameter sweeps should identify the exact ranges, number of grid points and threshold-crossing convention.

For $\beta_h = 0.15$ with $\beta_v = 0.40$, $\mu_h = 0.20$ and $\mu_v = 0.30$, $R_0 = 1$. This critical case approaches the disease-free boundary under the model's deterministic dynamics, but the convergence can be slower than in a strictly subcritical case. For $\beta_h = 0.30$, 0.60 and 0.90, the corresponding values are $R_0 = \sqrt{2}$, 2 and $\sqrt{6}$, respectively.

5.3 Elasticity and threshold requirements

The normalized forward sensitivity indices of R_0 are obtained by differentiating equation (2):

$$\Upsilon_{\beta_h}^{R_0} = \Upsilon_{\beta_v}^{R_0} = \frac{1}{2}, \quad \Upsilon_{\mu_h}^{R_0} = \Upsilon_{\mu_v}^{R_0} = -\frac{1}{2}. \tag{11}$$

Thus the local elasticity magnitudes are equal by construction. The reduced model alone cannot rank host-side and vector-side interventions without additional information about achievable intervention effects, costs, uncertainty and implementation constraints.

Holding the other baseline parameters fixed, the strict subcritical conditions are $\beta_h < 0.15$, $\beta_v < 0.10$, $\mu_h > 0.80$ or $\mu_v > 1.20$ when changing one parameter at a time. These are mathematical threshold calculations, not recommendations to change biological removal rates by those amounts.

5.4 Robust allocation scenarios

The nine allocations below are recomputed with constrained nonlinear optimisation; the objective is a synthetic relative-effort index, not measured monetary expenditure. Control caps are 0.95, the worst-case reproduction target is 0.95, and upper transmission bounds are multiplied by 1.0, 1.2 or 1.4. All reported solutions are checked for constraint feasibility and first-order stationarity. Numerical results should not be interpreted as field intervention recommendations.

Scenario	$c_□$	c_v	$u_□$	u_v	Worst-case R_c
Nominal	1	1	0.5250	0.5250	0.9500
Nominal	1	4	0.7631	0.0474	0.9500
Nominal	4	1	0.0474	0.7631	0.9500
Upper bounds +20%	1	1	0.6042	0.6042	0.9500
Upper bounds +20%	1	4	0.8376	0.0353	0.9500
Upper bounds +20%	4	1	0.0353	0.8376	0.9500
Upper bounds +40%	1	1	0.6607	0.6607	0.9500
Upper bounds +40%	1	4	0.8817	0.0268	0.9500
Upper bounds +40%	4	1	0.0268	0.8817	0.9500

© 2026 The Authors. Published by Bexford Publishing Ltd

Interpretation must remain conditional: increasing the relative cost weight for one control channel shifts the computed allocation toward the other channel, while larger uncertainty bounds generally require stronger suppression to preserve the same worst-case margin. These are model-based implications, not measured intervention effects.

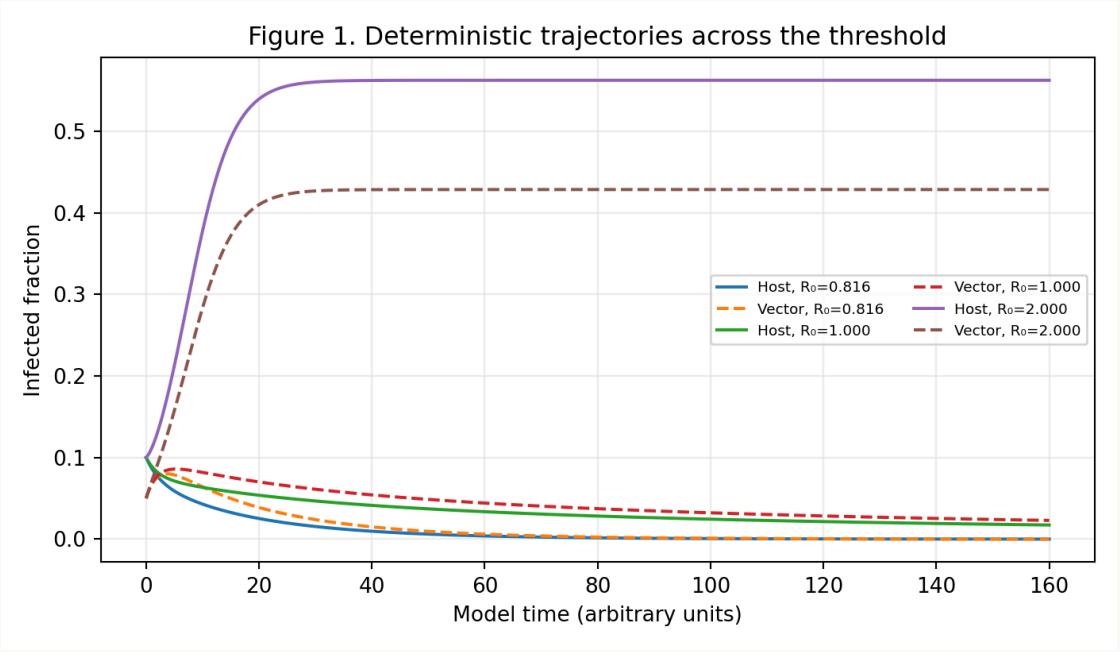
5.5 Numerical reproducibility and limitations

Computations use Python, SciPy solve_ivp (DOP853, relative tolerance 10^{-10}, absolute tolerance 10^{-12}) and scipy.optimize.minimize (SLSQP, ftol 10^{-12}). Initial infected fractions are x(0)=0.10 and y(0)=0.05; time is in arbitrary model time units because the illustrative rates are not calibrated. Each allocation is computed from multiple initial guesses. Constraint residuals and KKT stationarity checks are reported in the reproducibility supplement. No observational data, uncertainty estimation or independent external validation is claimed.

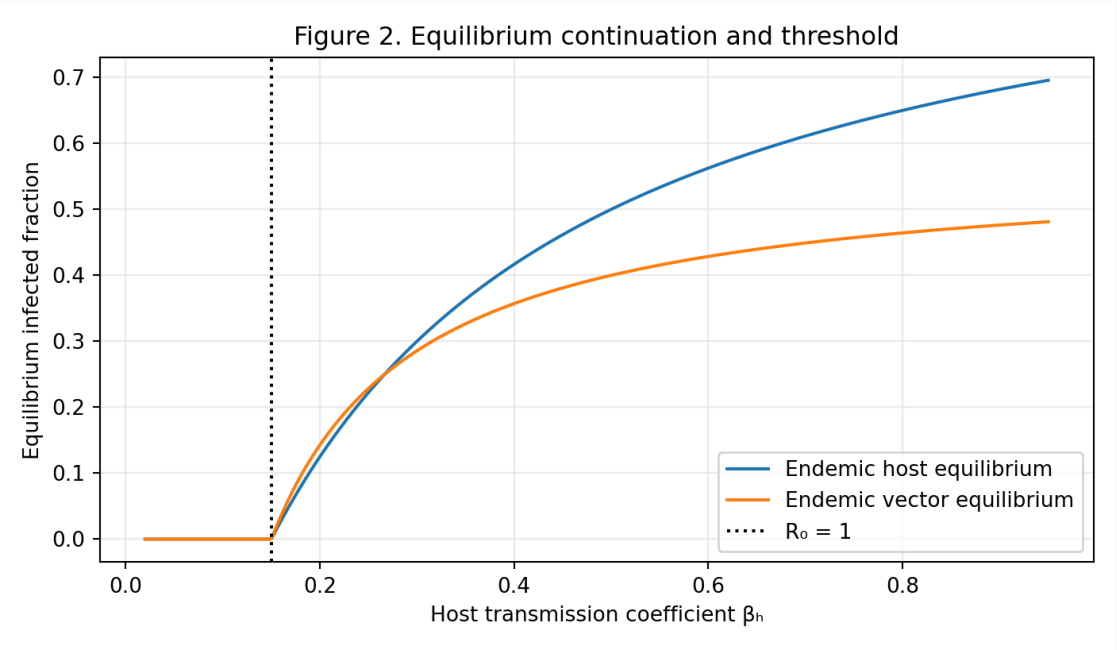
5.6 Independently generated numerical simulations

Figure 1 compares host and vector trajectories for β_h = 0.10, 0.15 and 0.60, with β_v = 0.40, μ_h = 0.20 and μ_v = 0.30. These correspond to $R_0 \approx 0.8165$, 1 and 2. Figure 2 traces the analytically derived equilibrium branches as β_h varies; Figure 3 shows control effort as uncertainty bounds increase. All figures are synthetic, with no fitted parameters.

Figure 1. Deterministic trajectories across the threshold



© 2026 The Authors. Published by Bexford Publishing Ltd



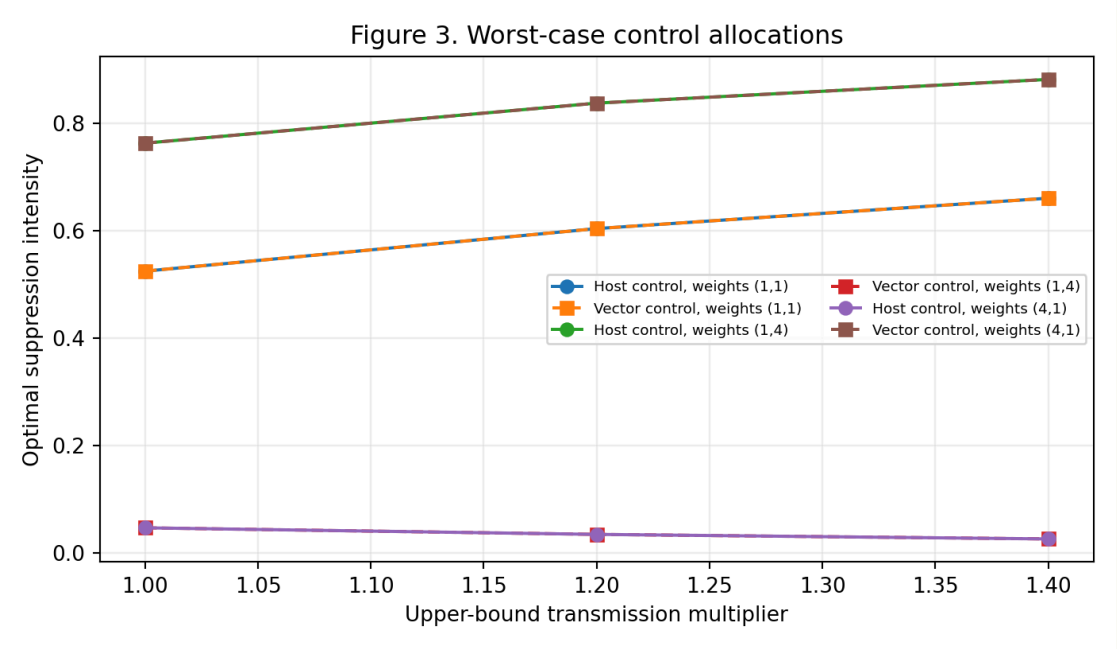


Table 2. Independently recomputed robust allocations (synthetic parameters).

Multiplier	c□	c_v	u□	u_v	Worst R_c	Effort	KKT norm
1.0	1	1	0.5250	0.5250	0.950000	0.54875	3.1e-16
1.0	1	4	0.7631	0.0474	0.950000	0.59138	2.2e-10
1.0	4	1	0.0474	0.7631	0.950000	0.59138	1.8e-14
1.2	1	1	0.6042	0.6042	0.950000	0.68663	0.0e+00
1.2	1	4	0.8376	0.0353	0.950000	0.70653	3.6e-15
1.2	4	1	0.0353	0.8376	0.950000	0.70653	2.9e-15
1.4	1	1	0.6607	0.6607	0.950000	0.76977	0.0e+00
1.4	1	4	0.8817	0.0268	0.950000	0.78029	3.8e-10

© 2026 The Authors. Published by Bexford Publishing Ltd

1.4	4	1	0.0268	0.8817	0.950000	0.78029	3.8e-10

All nine runs achieved worst-case $R_c \leq 0.950001$; maximum absolute constraint violation = 4.41e-14; maximum interior stationarity residual = 3.83e-10. These checks establish numerical feasibility and approximate first-order stationarity, not independent global optimality.

6. PROPOSED STOCHASTIC AND KOOPMAN-BASED EXTENSIONS

6.1 Candidate stochastic formulation

A possible stochastic extension is

$$dX_t = \left[\beta_h\left(1 - X_t\right)Y_t - \mu_h X_t\right]dt + \sigma_h X_t\left(1 - X_t\right)dW_1,$$
$$dY_t = \left[\beta_v\left(1 - Y_t\right)X_t - \mu_v Y_t\right]dt + \sigma_v Y_t\left(1 - Y_t\right)dW_2. \qquad (12)$$

Here W_1 and W_2 are independent standard Brownian motions and σ_h, $\sigma_v \geq 0$. The diffusion terms vanish at the boundary, but invariance of the square must be established under a precise stochastic viability argument. A complete stochastic analysis would separately address global existence, state-space invariance, extinction, persistence and the relation between noise intensity and threshold behaviour. None of these stochastic theorems is claimed as proved in this manuscript.

6.2 EDMD data and evaluation protocol

For observations z_k containing plant infection, infectious-vector prevalence and relevant covariates, form snapshot pairs (z_k, z_{k+1}) at a fixed sampling interval Δt. Select and document a dictionary $\psi(z)$, for example constant, linear, quadratic and biologically motivated cross terms. Define [8]

$$G = \frac{1}{M}\sum_{k=1}^{M}\psi\left(z_k\right)\psi\left(z_k\right)^T,$$
$$A = \frac{1}{M}\sum_{k=1}^{M}\psi\left(z_k\right)\psi\left(z_{k+1}\right)^T. \qquad (13)$$

The operator matrix depends on the chosen row/column convention for observables; this convention must be stated consistently before calculating eigenvalues, modes and forecasts. Regularization should be tuned using training-only validation. Chronological training, validation and test partitions should be used to avoid information leakage. [8]

Compare EDMD forecasts with persistence, deterministic ODE and, where appropriate, stochastic-ensemble baselines. Report one-step and multistep RMSE and MAE, and evaluate uncertainty calibration if predictive intervals are produced. No EDMD accuracy or superiority claim is made without a suitable observed dataset.

7. DISCUSSION

The independently generated trajectories support the analytical distinction between subcritical elimination, slow critical decay and convergence to a positive endemic equilibrium in the supercritical case. The equilibrium continuation identifies a forward threshold at $R_0=1$, while robust allocations show the trade-off between uncertainty size and relative effort costs. These conclusions are model-internal: the assumed constant total plant/vector populations and omission of infected cuttings are substantial limitations. In

© 2026 The Authors. Published by Bexford Publishing Ltd

particular, importing infected planting material can invalidate the disease-free equilibrium of the simplified model [3].

For fixed admissible transmission coefficients, the robust inequality yields a strict worst-case threshold for local stability and global elimination in the reduced model. The equality case deserves precision: the linearisation is non-hyperbolic, but the same LaSalle argument as in Section 3.5 establishes global disease-free stability for fixed nonnegative controlled transmission coefficients at equality. Thus strict inequality is necessary for uniform Hurwitz linearisation, not for nonlinear asymptotic stability at the critical threshold.

The numerical allocations depend on assumed effort weights, suppression caps and rectangular uncertainty bounds. Neither their empirical attainability nor their real costs have been measured. More realistic research should incorporate planting-material infection, seasonal vector dynamics, parameter identifiability, control-effect estimation and prospective field data. EDMD forecasting must remain a separate validated study rather than an implied result of these synthetic ODE simulations.

8. CONCLUSION

This study establishes analytical threshold properties for a reduced cassava host–vector system and supplies reproducible synthetic tests of trajectories, equilibrium continuation and nine robust control allocations. The model predicts elimination for $R_0 \leq 1$ and a unique locally stable endemic equilibrium for $R_0 > 1$. Robust allocation demonstrates how worst-case uncertainty and relative effort weights alter mathematically feasible control combinations. These findings are not estimates of actual CMD incidence or intervention efficacy. Field-calibrated transmission, infected-cutting importation and independent forecast evaluation are required before operational recommendations can be made.

References

[1] Chikoti, P. C., & Tembo, M. (2022). Expansion and impact of cassava brown streak and cassava mosaic diseases in Africa: A review. Frontiers in Sustainable Food Systems, 6, 1076364. https://doi.org/10.3389/fsufs.2022.1076364

[2] Erick, B., & Mayengo, M. (2022). Modelling the dynamics of cassava mosaic disease with non-cassava host plants. Informatics in Medicine Unlocked, 33, 101086. https://doi.org/10.1016/j.imu.2022.101086

[3] Jittamai, P., Chanlawong, N., Atisattapong, W., Anlamlert, W., & Buensanteai, N. (2021). Reproduction number and sensitivity analysis of cassava mosaic disease spread for policy design. Mathematical Biosciences and Engineering, 18(5), 5069–5093. https://doi.org/10.3934/mbe.2021258

[4] Lusekelo, E., Helikumi, M., Daudi, S., & Mushayabasa, S. (2025). Optimal control applied to a stage-structured cassava mosaic disease model with vector feeding behavior. Results in Control and Optimization, 18, 100522. https://doi.org/10.1016/j.rico.2025.100522

[5] Sangsawang, S., Humphries, U., Khan, A., & Pongsumpun, P. (2024). Sensitivity analysis and optimal control for the dynamic mathematical model of cassava mosaic disease. AIP Advances, 14, 065230. https://doi.org/10.1063/5.0207497

[14] Spatial dynamics and control of a crop pathogen with mixed-mode transmission. (2017). PLOS Computational Biology. doi:10.1371/journal.pcbi.1005654. [Verify author metadata before submission.]

© 2026 The Authors. Published by Bexford Publishing Ltd

[13] Oh, M., & Garg, M. (2025). Modeling partial cross-protection for managing cassava mosaic disease: A vector–host framework and sensitivity analysis. Frontiers in Agronomy, 7, 1701543. doi:10.3389/fagro.2025.1701543.

[6] Chavez, V. A., Milne, A. E., van den Bosch, F., Pita, J., & McQuaid, C. F. (2022). Modelling cassava production and pest management under biotic and abiotic constraints. Plant Molecular Biology, 109, 325–349. https://doi.org/10.1007/s11103-021-01170-8

[7] Modeling, analysis, and transmission dynamics of cassava mosaic disease through stochastic fractional delay differential equations. (2025). Mathematics, 13(3), 383. https://doi.org/10.3390/math13030383. [Verify full author metadata before submission.]

[8] Williams, M. O., Kevrekidis, I. G., & Rowley, C. W. (2015). A data-driven approximation of the Koopman operator: Extending dynamic mode decomposition. Journal of Nonlinear Science, 25(6), 1307–1346. https://doi.org/10.1007/s00332-015-9258-5

[9] Ogoegbulem, O., Ochonogor, N. I., Njoseh, I. N., & Abanum, G. C. (2024). Mathematical analysis of a real time dynamical system: Interaction between agricultural variables. Scientific African.

[10] Iweobodo, D. C., Abanum, G. C., Ochonogor, N. I., Apanapudor, J. S., & Njoseh, I. N. (2024). A Galerkin finite element technique with Iweobodo–Mamadu–Njoseh wavelet (IMNW) basis function for the solution of time-fractional advection–diffusion problems. Partial Differential Equations in Applied Mathematics, 12, 100965. https://doi.org/10.1016/j.padiff.2024.100965

[11] Ochonogor, N. I., Okonye, A. O., Obukohwo, V., & Akpobroka, I. B. (2023). One dimensional torus. IOSR Journal of Mathematics, 19(6), 30–35. [Verify title capitalization and publication metadata.]

[12] Ochonogor, N. I., & Okonye, A. O. (2026). Measure preserving transformations: Theory, examples and applications. Global Academic and Scientific Journal of Multidisciplinary Studies, 4(1), 12–17. https://doi.org/10.5281/zenodo.18133396. [Verify final publication record.]

[13] Ochonogor, N. I., Nduka, G. S., & Egbogho, H. E. (2026). A nonlinear ordinary differential equation model for the effects of fasting on the human body system. SSR Journal of Multidisciplinary (SSRJM), 3(10), 1-16.

[14] Oghenerhoro, S. P., Nduka, G. S., Ogoegbulem, O., Egbogho, H. E., Akpobroka, B. I., & Emunefe, F. G. (2026). Algorithmic Modeling and Simulation of Non-Carcinogenic Health Risk from Black Soot Exposure among Population Groups in Warri Metropolis, Nigeria. Tech-Sphere Journal for Pure and Applied Sciences, 3(1), 94-107.

© 2026 by the authors. Submitted for possible open access publication under the terms and conditions of the **Creative Commons Attribution (CC BY 4.0) licence** (https://creativecommons.org/licenses/by/4.0/)